Journal of Innovation and Development
ISSN: 2958-4752 | Vol. 15, No. 3, 2026

Bionic Parameter Extraction for Robotic Fish Design: A Reverse-Engineering Approach Using Large Yellow Croaker

Zhixin Wang[1, a]

[1]Xihua University, Chengdu, Sichuan 610039, China
[a]fiherywang@gmail.com

Abstract: The bionic research on fish swimming is the theoretical basis for the design of robotic fish. Accurately extracting the parameters of the fish body wave equation is the key to achieving efficient biomimetic motion. This study adopted an innovative reverse parameter extraction method to accurately quantify the hydrodynamic characteristics of fish swimming based on real biological fish motion data. Five adult yellow croakers (*Larimichthys crocea*) were selected as experimental subjects. Continuous video capture was conducted for 7 hours at a sampling rate of 30 fps in a constant-temperature two-dimensional water environment. By utilizing OpenCV digital image processing technology, an automatic extraction workflow was established to convert the original video into the centerline of the fish body, including key steps such as grayscale conversion and skeleton extraction. On this basis, using the Lighthill slender body theory framework, the key parameters in the fish wave equation were accurately determined through point marking, coordinate transformation, and discrete fitting methods. The experimental results show that the tail beat period of the large yellow croaker is 0.5s (frequency f=2Hz), the maximum amplitude of tail beat A is 3.25cm, and the amplitude to body length ratio is $2A/L \approx 0.19$, which conforms to biological laws; The average swimming speed U is 13.3cm/s, with a slip ratio of 0.86, which is in line with theoretical expectations; The parameters of the fish body wave equation obtained through envelope fitting are C_1=-0.075, C_2=0.5, k=10, and $\omega=4\pi$. The waveform reconstructed based on these parameters in MATLAB has high similarity with the actual swimming motion of the large yellow croaker, verifying the accuracy of the fitting. The fish body wave parameters obtained by this method lay a reliable biological foundation for the subsequent precise design of the robotic yellow croaker.

Keywords: Large yellow croaker; fish body wave equation; digital image processing; parameter extraction; biomimetic robotic fish.

1. Introduction

The development of underwater robots and biomimetic robotic fish has led to progress in robotics, ocean engineering and biomimetic design. Compared with the traditional propeller drive system, the propulsion mechanism based on fish motion has higher energy conversion efficiency, stronger maneuverability and better environmental adaptability. Therefore, describing the hydrodynamic mechanism of fish swimming naturally and accurately extracting the critical motion parameters of fish are the premise of robotic fish design. Large yellow croaker*(Larimichthys crocea)* is a long-distance migratory fish. It exhibits a typical crucian carp shaped swimming mode. It uses body and tail fin (BCF) propulsion to achieve the best balance between speed and agility. It is an ideal bionic research object.

Breder (1926) initiated the systematic classification of fish movement, adding the suffix "-iform" to the terminology of Ichthyology to indicate different propulsion modes [1]. This work laid the foundation for subsequent kinematic analyses. Lindsey (1978) greatly expanded Breder's framework [2], which was later further improved by Webb and Blake (1984) [3]. A major contribution of Lindsey's work is to subdivide the body and caudal fin (BCF) propulsion fish into four different modes: Anguilliform mode: The entire body participates in wave propagation with amplitude increasing along body length and elevated oscillation frequency; Subcarangiform mode: The anterior body remains relatively rigid, with wave generation primarily from posterior segments; Carangiform mode: Pronounced wave formation occurs only in the caudal region, while the trunk maintains relative stability; Thunniform mode: Propulsion derives primarily from caudal fin oscillation, with the body maintaining a nearly straight configuration[2].

In 1999, Sfakiotakis further developed a two-dimensional classification framework based on the basic work of Lindsey [4]. The system organizes the movement of fish through two independent dimensions. The first dimension classifies the types of propulsion mechanism, distinguishing BCF (body and caudal fin propulsion) and MPF (median fin and paired fin propulsion). The propulsion of BCF (body and caudal fin propulsion) comes from the coordinated movement of body and caudal fin, and the whole hind body participates in the propulsion movement. The propulsion of MPF (median fin and paired fin propulsion) comes from the oscillation or fluctuation of median fin (dorsal fin and anus) and paired fin (pectoral fin and pelvis), while the trunk remains relatively rigid. The second dimension classifies the body deformation patterns. Wave represents a mode in which the propulsion mechanism produces continuous traveling waves propagating along the length of the body. Taking eel (Anguilliformes) and ray (rays) as examples, continuous body segments undergo coordinated lateral displacement to form a characteristic S-shaped structure. On the contrary, oscillation represents the mode in which the propulsion mechanism performs rotational motion around its base, generating thrust through oscillatory motion, while the rest of the body area remains relatively stable; This model is characterized by winged swimmers and

species that rely mainly on caudal fin propulsion[5]. The combination of BCF and fluctuation is adopted by the large yellow croaker to represent an intermediate movement strategy to achieve a balance between energy efficiency and operability.

2. Theoretical Foundation

In order to systematically analyze the hydrodynamic forces on fish bodies, Lighthill (1960s) innovatively proposed the slender body theory [6,7], which is applicable to the case where the lateral body change can be ignored relative to the longitudinal changes, and allows the hydrodynamic modeling through the slender body approximation.

The theory is based on the following basic assumptions:

(1) Relative to the longitudinal change, the lateral body change can be ignored, so as to achieve the slender body approximation;

(2) The cross-sectional characteristics of the fish were analyzed, and only the tail participated in the oscillatory motion;

(3) Analysis requires sufficiently high Reynolds numbers, typically within the range $\boldsymbol{Re = 10^4 - 10^8}$;

(4) The water flow around the fish body constitutes a steady state condition;

(5) Lateral body displacement caused by approaching water flow $\boldsymbol{h(x,t)}$.

The core concept of the theory is rooted in the principle of kinetic energy and momentum, and it is assumed that the hydrodynamic force is completely dependent on the cross-sectional flow parameters of the moving afterbody segment. In the Lighthill framework, when the fish accelerate, they also change the momentum of the surrounding fluid. This momentum component is called added mass momentum, which reflects the inertial effect of fluid.

The added mass momentum per unit length represents the product of virtual mass and velocity. The time rate of change of the added mass momentum per unit length is equal to the hydrodynamic force exerted by the fluid on the fish. The additional mass momentum expression of Lighthill is:

$$\boldsymbol{\rho V(x,t)A(x)} \qquad (1)$$

where $\boldsymbol{\rho}$ denotes fluid density, $\boldsymbol{V(x,t)}$ represents virtual velocity, and $\boldsymbol{A(x)}$ is the cross-sectional area at position $\boldsymbol{x}$.

The time derivative of the added mass momentum represents the force exerted by the fish on the surrounding waters; On the contrary, the reaction force of water on fish is:

$$\boldsymbol{L(x,t) = -\rho\left(\frac{\partial}{\partial t} + U\frac{\partial}{\partial x}\right)[V(x,t)A(x)]} \qquad (2)$$

In the framework of slender body, Taylor proposed the relationship between virtual velocity and swimming velocity, and obtained the empirical value $\boldsymbol{V/U \approx 0.7}$. Subsequently, Taylor[8] developed an early kinematic model:

$$\boldsymbol{y = B\sin\frac{2\pi}{\lambda}[x + (U - V)t]} \qquad (3)$$

where $\boldsymbol{B}$ denotes amplitude, $\boldsymbol{\lambda}$ represents wavelength, $\boldsymbol{U}$ is wave propagation speed, and $\boldsymbol{V}$ is swimming speed.

In 1960, Lighthill formulated the classical expression for fish body waves:

$$\boldsymbol{h(x,t) = f(x)g\left(t - \frac{x}{c}\right)} \qquad (4)$$

This spatiotemporal displacement function encompasses position variable $\boldsymbol{x}$ and time variable $\boldsymbol{t}$.

Where $\boldsymbol{g(t)}$ is the oscillation component (trigonometric function), $\boldsymbol{c}$ is the wave propagation velocity along the surface of the fish body, and$\boldsymbol{f(x)}$ is the envelope function describing the amplitude change along the length of the fish body. It is then called fish body wave, which describes the sinusoidal body deformation generated in the process of motion. The fish body wave propagates backward, pushing the fish forward in the water.

According to the experimental observations of Videler[9-12] and his colleagues on Atlantic cod and mackerel, Borazjani[13] described the envelope function of carangiform fish as a quadratic polynomial:

$$\boldsymbol{a(x) = a_0 + a_1x + a_2x^2} \qquad (5)$$

In contemporary engineering applications, the fish body wave equation has evolved into its standard form:

$$\boldsymbol{f(x,t) = (C_1x + C_2x^2)\sin(kx + \omega t)} \qquad (6)$$

The expression plays a key role in robot fish motion control. The physical interpretation of the parameters is as follows: $\boldsymbol{C_1}$ represents the linear envelope coefficient, reflecting the amplitude variation along the body length; $\boldsymbol{C_2}$ refers to the secondary envelope coefficient and nonlinear amplitude modulation; $\boldsymbol{k}$ is the wave number ($\boldsymbol{k = 2\pi/\lambda}$), which is relatively simple to determine for multiple wavelengths observed in species such as Anguilliformes; $\boldsymbol{\omega}$ is the angular frequency, defined as $\boldsymbol{\omega = 2\pi f}$ where f is the tail beat frequency.

In practical observation and engineering application, it is still a challenge to obtain complete and accurate wave equation of fish body. Therefore, researchers usually use the existing empirical formula or the established parameter set as table 1 [14].

Table 1. The common number of simulation

	Anguilliform mode	Subcarangiform mode	Carangiform mode	Thunniform mode
C_1	1.0	0.7	0.4	0.1
C_2	0.0	0.3	0.6	0.9
λ	0.5	0.75	1.0	1.25
V	1.02	1.35	1.43	1.36

However, these empirical parameters show obvious limitations. On the one hand, these parameters mainly come from the observation of specific fish species under specific environmental conditions; There may be significant differences among different species, individual specimens and fish in different physiological states. Therefore, the applicability of these parameters to different motion environments is still limited. On the other hand, the traditional parameter design to refine the workflow will lead to low efficiency in the development of robotic fish, which needs iterative modification to obtain satisfactory bionic performance. This iterative method not only prolongs the design cycle, but also introduces a lot of uncertainties in the process of engineering optimization.

3. Materials and Methods

3.1. Specimen Selection and Experimental Setup

3.1.1. Experimental Subjects

This study employed five adult specimens of large yellow croaker(*Larimichthys crocea*)as experimental subjects. All experimental fish were cultured artificially, and appropriate domestication training was conducted before data collection to minimize stress-induced behavioral abnormalities.

The experimental device used the two-dimensional observation environment of fixed position overhead imaging to ensure that the fish swimming plane is parallel to the camera imaging plane. This structure facilitates the subsequent two-dimensional image analysis.

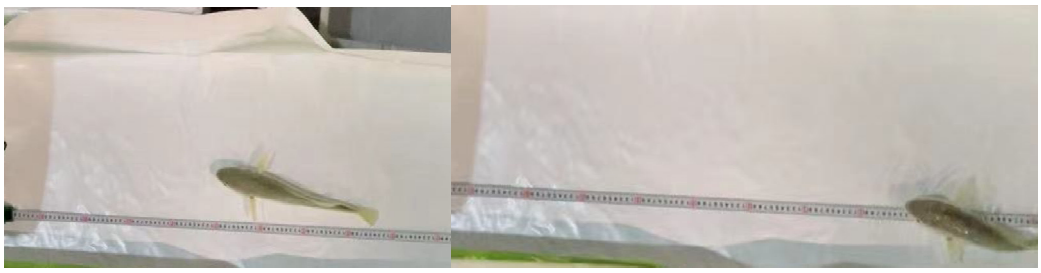

Figure 1. Measurement environment in two-dimensional environment

3.1.2. Data Acquisition Specifications

The data were collected under standardized conditions to ensure the reproducibility of the experiment. Continuous video capture over 7 hours provided a comprehensive data set of swimming behavior under natural conditions. Keeping the sampling rate at 30 frames per second (FPS) is enough to solve the tail shot kinematics without excessive computational requirements. In order to eliminate the influence of thermal effect on the motion behavior of fish, the experimental environment was kept at a constant temperature in a two-dimensional water tank. In order to minimize human interference, the experimental personnel immediately vacate the acquisition area after completing the video acquisition, so as to reduce the behavior changes caused by human presence.

3.2. Image Processing Workflow

3.2.1. Grayscale Conversion and Image Preprocessing

Collect original video frames in color RGB format. In order to facilitate the subsequent feature extraction, the original image is grayscale converted, and the three channel RGB image is converted to a single channel grayscale representation. The standard conversion formula adopted is:

$$\text{Gray} = \mathbf{0.299} \times \boldsymbol{R} + \mathbf{0.587} \times \boldsymbol{G} + \mathbf{0.114} \times \boldsymbol{B}$$

This formulation assigns differential weighting to individual color channels, enabling the converted grayscale values to preserve visual features from the original image more effectively than simple channel averaging.

3.2.2. Skeleton Extraction Algorithm

In order to extract the centreline of fish accurately, a skeleton extraction algorithm is implemented. The basic principle of the algorithm is to gradually erode from the edge of the target object until it reaches the center. The specific processing protocol includes the following steps: (1) establishing a $\mathbf{3} \times \mathbf{3}$ pixel sliding window centered on each target pixel; (2) The target is etched and refined step by step according to the pixel characteristics in the window; (3) Continue to erode until the skeleton width is reduced to a single pixel width; (4) The resulting single pixel sequence that forms the centerline of the fish body. The implementation is completed using the skeleton extraction functions available in the OpenCV library. Because the accuracy of skeleton extraction directly affects the subsequent waveform analysis, the iterative verification program is used in the whole implementation process to ensure the accuracy.

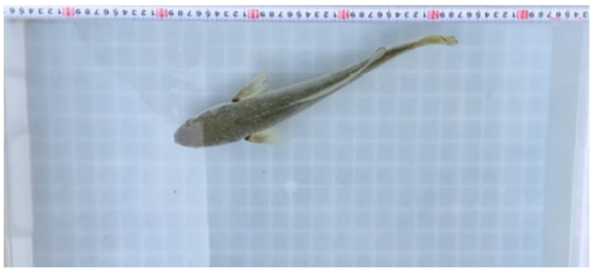

Figure 2. Original picture of large yellow croaker

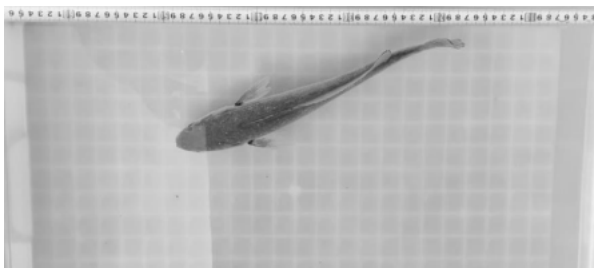

Figure 3. Grayscale map of large yellow croaker

Figure 4. The centerline of the fish body in one frame of image

3.3. Fish Body Wave Reconstruction

The virtual pointer interface established in OpenCV is used to mark the fish waveform image with discrete boundary points. The coordinate data obtained is exported in comma separated value (CSV) format to support subsequent quantitative analysis.

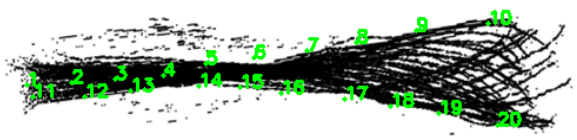

Figure 5. Solve the envelope equation fixed point

In the process of waveform reconstruction, special attention should be paid to coordinate system conversion. The local OpenCV coordinate system displays the reverse Y-axis direction relative to the standard Cartesian coordinates in the mathematical convention, and coordinate transformation is required for correction. In addition, interpolation algorithm is used to generate smooth waveform contour for discrete point data, which enhances the geometric fidelity of waveform contour.

4. Results

4.1. Fish Body Wave Characteristics Analysis

4.1.1. Tail-Beat Period and Frequency

Through systematic observation of multiple complete tail beat cycles of large yellow croaker, the tail beat characteristics of large yellow croaker were determined. A complete tail beat period is defined as the process in which the tail fin leaves the neutral position, passes through the maximum displacement position (dorsal and ventral) in turn, and then returns to the neutral position.

Observations revealed that the large yellow croaker required approximately 0.5 seconds to complete a single tail-beat cycle, corresponding to a tail-beat frequency of $\boldsymbol{f = 2\ Hz}$. The frequency showed good stability in multiple samples and over a long observation period. Compared with the high-frequency oscillatory swimming animals such as eels, the relative low-frequency characteristics of large yellow croaker reflect its motion characteristics as a crucian carp. The frequency range of eels is 5~10 Hz. This frequency is consistent with the characteristics of tuna's intermediate motion strategy, which represents the tradeoff between the extreme body fluctuation of eels and the rigid body oscillation of tuna.

Figure 6. Swimming posture of large yellow croaker in one second

4.1.2. Quantitative Measurement of Caudal Amplitude

To minimize single-measurement errors, caudal amplitude data were collected across multiple tailbeat cycles from individual specimens and subsequently averaged. The maximum caudal amplitude was defined as $\boldsymbol{A}$, representing the maximum perpendicular distance of the caudal fin from the body's longitudinal centerline.

Measurement results yielded the following values: maximum caudal amplitude $\boldsymbol{A = 3.25\ cm}$; the amplitude parameter employed in Strouhal number calculations, $\boldsymbol{Ah \approx 6.5\ cm}$; specimen total body length $\boldsymbol{L = 36\ cm}$; and the amplitude-to-body-length ratio $\boldsymbol{2A/L \approx 0.19}$. This ratio precisely conforms to the empirically established relationship from prior research indicating that fish tail-beat amplitude approximates 0.2 times body length. This quantitative correspondence not only validates the accuracy of the digital image processing methodology but also confirms the efficacy of the skeleton extraction algorithm in capturing fish body geometric characteristics with high fidelity.

4.2. Swimming Speed Measurement and Calculation

4.2.1. Acquisition of Swimming Velocity

Through the displacement measurement based on video frame sequence, the accurate measurement of swimming speed is realized. The operation scheme is as follows: (1) in the process of data acquisition, the calibration scale is pasted on the side wall of the aquarium to establish the reference standard for pixel to physical distance conversion; (2) Extracting the horizontal coordinate position of the fish head (or the center of the fish body) from the continuous video frames; (3) Using 30 FPS sampling rate and scale reference data, the forward displacement of the fish in the known time interval was calculated; (4) The swimming speed is determined by u=displacement/elapsed time.

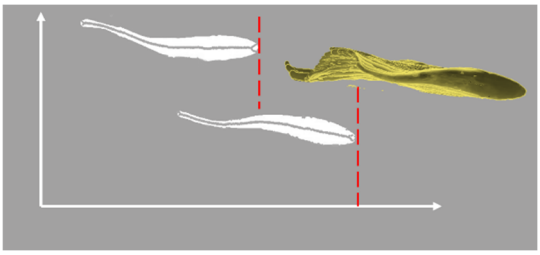

Figure 7. Schematic diagram of the calculation of fish swimming speed U

A key methodological consideration is that the speed calculation only includes the swimming state showing obvious tail beat motion, and explicitly excludes the state

where the slip rate is equal to a unit ($\boldsymbol{U = V}$, indicating body drift without active tail motion). This selective approach ensures that the measured speed represents active swimming performance rather than passive drift.

4.2.2. determination of slip ratio

Slip ratio refers to the ratio of swimming speed to wave propagation speed, which is an important index to measure the propulsion efficiency. Using the same measurement protocol, quantify the velocity in the passive drift state (where no tail beat motion occurs, only trunk drift continues), and obtain the slip velocity $\boldsymbol{V}_{\text{slip}}$.

The results show that the slip velocity $\boldsymbol{V}_{\text{slip}} = \mathbf{15\ cm/s}$; active swimming velocity $\boldsymbol{U} = \mathbf{13.3\ cm/s}$; and slip ratio $= \boldsymbol{U/V}_{\text{slip}} = \mathbf{13.3/15 = 0.86}$. This value precisely falls within the empirical range predicted by Lighthill slender-body theory, specifically $\boldsymbol{V/U \approx 0.7 \pm 0.15}$ (corresponding to $\mathbf{0.55 - 0.85}$), which proves that the measurement method and parameter calculation are highly consistent with the established hydrodynamic principles.

4.3. Fish Body Wave Equation Parameter Extraction

4.3.1. Envelope Function Determination

The fish body waveform image represents a composite representation of the body centerline configuration throughout the oscillation period. In order to accurately fit the coefficients $\boldsymbol{C_1}$ and $\boldsymbol{C_2}$ in the envelope equation, the following systematic methods are used: first, 20 discrete marker points are selected on the fish waveform image, and their pixel coordinates are obtained through the OpenCV virtual pointer interface. Secondly, coordinate system conversion is performed by using the calibrated proportional reference to convert the pixel coordinates to physical coordinates (centimeters), and correct the direction difference between the OpenCV coordinate system and the standard mathematical Cartesian coordinates. Thirdly, the equations are constructed and solved according to the theoretical form of envelope function.

4.3.2. Solution of Coefficients $\boldsymbol{C_1}$ and $\boldsymbol{C_2}$

The analysis of the distribution of marker points reveals the significant geometric characteristics of a specific location. Points $1 - 6$ and $11 - 16$ are located in the relatively flat area of the envelope, while points 10 and 20 are located at the position of the maximum amplitude during body swing, representing the extreme value of the envelope function. These extremum constraints are used to construct binary equations. It is worth noting that the coordinate values in the solution process are in meters (m) to ensure that the size is consistent with the standard form of the wave equation.

Based on the envelope function $\boldsymbol{a(x) = C_1 x + C_2 x^2}$ and the constraints imposed by extremal points, algebraic solution yielded: $\boldsymbol{C_1 = -0.075}$ and $\boldsymbol{C_2 = 0.5}$.

4.3.3. Complete Fish Body Wave Equation

Integrating all extracted parameters, the complete fish body wave equation for the large yellow croaker is expressed as:

$$\boldsymbol{f(x,t) = (-0.075x + 0.5x^2)\sin(10x + 4\pi t)}$$

where the wavenumber $\boldsymbol{k = 10}$, angular frequency $\boldsymbol{\omega = 4\pi rad/s}$, and the envelope function coefficients are $\boldsymbol{C_1 = -0.075}$ and $\boldsymbol{C_2 = 0.5}$. Numerical reconstruction of this equation in the MATLAB environment generated waveforms exhibiting high correspondence with the actual swimming postures of the large yellow croaker, providing substantial validation of parameter fitting accuracy.

4.3.4. Verification of Parameter Fitting Precision

In order to evaluate the accuracy of the extracted parameters, a comprehensive validation strategy was implemented. In the MATLAB computing environment, the extracted parameters are used to reconstruct the fish body waveform, and compared with the original experimental data. The reconstructed waveform is consistent with the swimming trajectory and body height of the actual fish, which verifies that the envelope coefficients ($\boldsymbol{C_1, C_2}$) have good fitting accuracy, and the frequency and wave values are appropriate, which verifies the effectiveness of the overall equation. These results verify that the extracted parameters accurately reflect the hydrodynamic and kinematic characteristics of large yellow croaker.

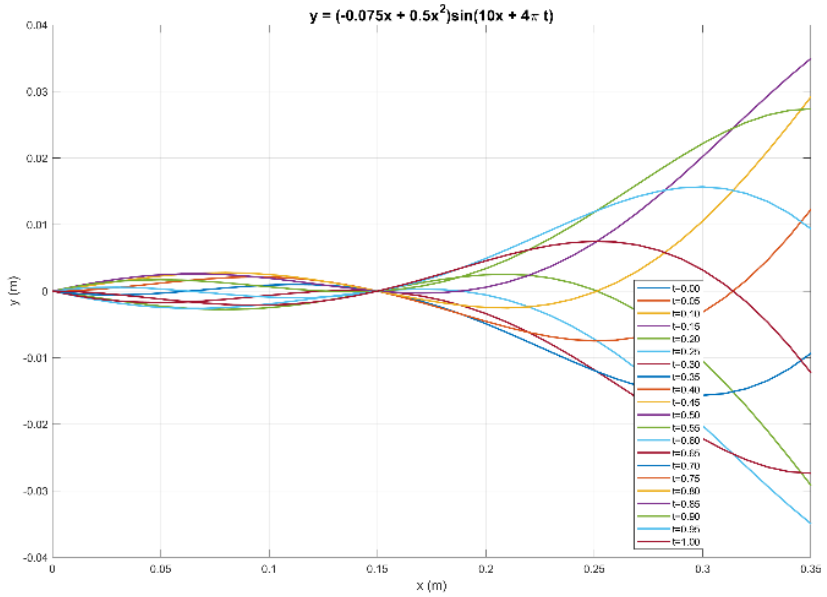

Figure 8. The fish traveling-wave by matlab

5. Discussion

5.1. Validation of Caudal Amplitude Measurements

In this study, the maximum amplitude of the tail fin of large yellow croaker was measured as $\mathbf{A = 3.25\ cm}$, and the ratio of amplitude to body length was $\boldsymbol{2A/L \approx 0.19}$, which fully conformed to the empirical rule established in previous studies that "the amplitude of the tail beat is usually about 0.2 times the body length".

5.2. Analysis of Tail-Beat Frequency and Swimming Kinematics

Through the systematic observation of multiple tail beat periods, it was determined that the tail beat frequency of the large yellow croaker was stable at 2 Hz and the constant period was 0.5 s. This frequency value was consistent with the biological characteristics of medium speed swimming of the large yellow croaker. Compared with the high-frequency oscillator with the same frequency of 5 − 10 Hz in eels, the relatively low frequency observed in large yellow croaker reflects its kinematic characteristics as a scale swimmer. This difference reflects the evolutionary adaptation of different fish species to their respective niches and swimming patterns.

5.3. Assessment of Swimming Velocity and Slip Ratio

The average swimming velocity obtained in this study was $\mathbf{U = 13.3\ cm/s}$. When combined with the calculated slip velocity of $\boldsymbol{V_{slip} = 15\ cm/s}$, the resulting slip ratio of 0.86 precisely aligns with the empirical range of $\mathbf{V/U \approx 0.7 \pm 0.15}$ predicted by Lighthill's slender-body theory, thereby demonstrating high consistency between our measurement methodology and theoretical framework predictions.

The slip ratio obtained in this study is in good agreement with the previously estimated range reported in the literature. Previous studies have shown that 1-year-old large yellow croaker can maintain a speed of $\mathbf{30 - 60\ cm/s}$ for extended durations [16]. The swimming speed obtained in this experiment has a considerable deviation from these reported values. However, this difference can be attributed to several experimental conditions: after long-distance transportation, the samples of large yellow croaker are in hibernation state, with little feeding activity, leading to the natural reduction of metabolic activity. In addition, the measurement is carried out without external stimulation, which represents the swimming speed during free and relaxed exercise, rather than escape or migration behavior. Under the condition of migration or escape, the swimming speed of large yellow croaker will greatly exceed the value obtained in this controlled laboratory environment.

6. Conclusions

Through the systematic analysis of the swimming data of large yellow croaker with natural behavior, the complete parameter expression of the wave equation of the fish body was successfully extracted. These parameters reflect the real hydrodynamic characteristics of large yellow croaker in unrestricted swimming, and provide a scientific basis for the design of the bionic large yellow croaker robot. Compared with the method using general empirical parameters, the species-specific parameters derived in this study can significantly enhance the fidelity of bionics. By combining biological observation with engineering application, this study established the key link between biological science and precision bionic robot design. The obtained quantitative parameters, the developed calculation tools and the methods verified in the whole research process constitute a reliable scientific basis for the subsequent fish simulation research and the development of autonomous underwater vehicles. We believe that the bionic robot large yellow croaker constructed on the framework established in this paper will obtain the motion performance close to its biological counterpart, so as to realize the practical application in marine environment monitoring, intelligent aquaculture system and related underwater engineering.

References

[1] Breder, C. M. (1926). The locomotion of fishes. *Zoologica*, *4*. https://doi.org/10.5962/p.203769.

[2] Lindsey, C. C. (1978). Form, function, and locomotory habits in fish. *Fish Physiology*, *7*, 1–100. https://doi.org/10.1016/S1546-5098(08)60163-6

[3] Webb, P. W. (1984). Form and function in fish swimming. *Scientific American*, *251*(1), 72–82. https://doi.org/10.1038/scientificamerican0784-72

[4] Sfakiotakis, M., Lane, D. M., & Davies, J. B. C. (1999). Review of fish swimming modes for aquatic locomotion. *IEEE Journal of Oceanic Engineering*, *24*(2), 237–252. https://doi.org/10.1109/48.757275

[5] Smits, A. J. (2019). Undulatory and oscillatory swimming. *Journal of Fluid Mechanics*, *874*. https://doi.org/10.1017/jfm.2019.284

[6] Lighthill, M. J. (1960). Note on the swimming of slender fish. *Journal of Fluid Mechanics*, *9*(2), 305–317.

[7] Lighthill, M. J. (1971). Large-amplitude elongated-body theory of fish locomotion. *Proceedings of the Royal Society of London. Series B, Biological Sciences*, *179*(1055), 125–138.

[8] Taylor, G. (1952). Analysis of the swimming of long and narrow animals. *Proceedings of the Royal Society of London A*, *214*(1117), 158–183. https://doi.org/10.1098/rspa.1952.0159

[9] Videler, J. J., & Wardle, C. S. (1991). Fish swimming stride by stride: Speed limits and endurance. *Reviews in Fish Biology & Fisheries*, *1*(1), 23–40. https://doi.org/10.1007/BF00042660

[10] Wardle, C. S., Videler, J. J., & Altringham, J. D. (1995). Tuning in to fish swimming waves: Body form, swimming mode and muscle function. *Journal of Experimental Biology*.

[11] Videler, J. J. (1980). *Fish swimming*.

[12] Videler, J. J., & Hess, F. (1984). Fast continuous swimming of two pelagic predators, saithe (*Pollachius virens*) and mackerel (*Scomber scombrus*): A kinematic analysis. *Journal of Experimental Biology*, *109*, 209. https://doi.org/10.1242/jeb.109.1.209

[13] Borazjani, I., & Sotiropoulos, F. (2008). Numerical investigation of the hydrodynamics of carangiform swimming in the transitional and inertial flow regimes. *Journal of Experimental Biology*, *211*(Pt 10), 1541–1558. https://doi.org/10.1242/jeb.015644

[14] Du, R., Li, Z., & Wang, S. (2015). *Robot fish: Bio-inspired fishlike underwater robots*. Springer.

[15] Qashlim, A., Basri, B., & Haeruddin, H. (2020). Smartphone technology applications for milkfish image segmentation using OpenCV library. *International Journal of Interactive Mobile Technologies (iJIM)*, *14*(8), 150. https://doi.org/10.3991/ijim.v14i08.12423

[16] Zeng, J., Long, F., & Wang, J. (2022). GWAS reveals heritable individual variations in the inherent swimming performance of juvenile large yellow croaker. *Aquaculture*, *559*. https://doi.org/10.1016/j.aquaculture.2022.738419